Journal of Coastal Research	15	4	884–891	Royal Palm Beach, Florida	Fall 1999

Analysis of Oceanic Internal Waves from Airborne SAR Images

Xiaofeng Li†, John Morrison†, Leonard Pietrafesa†, and Andy Ochadlick‡

†Department of Marine,
Earth and Atmospheric
Sciences
North Carolina State
University
Raleigh, NC 27695, USA

‡Science Dimension
4476 Tollgate Road
New Hope, PA 18938, USA

ABSTRACT

LI, X.; MORRISON, J.; PIETRAFESA, L., and OCHADLICK, A., 1999. Analysis of Oceanic Internal Waves from Airborne SAR Images. *Journal of Coastal Research*, 15(4), 884–891. Royal Palm Beach (Florida), ISSN 0749-0208.

Two airborne Synthetic Aperture Radar (SAR) images, which were taken during Office of Naval Research High Resolution Ocean Experiment, were used to study internal wave characteristics along the continent shelf off Cape Hatteras, North Carolina on September 16, 1991. These images showed a mixed signal of oceanic internal waves and bottom sand waves. We interpreted the internal wave packet with wavelengths of about 270 m, which was comparable to the sand wave wavelength. Repeat images, taken together with *in situ* observations, indicated that the wave packet was propagating with the mean flow at a depth of about 9 meters. Coincident oceanographic measurements were used to determine the oceanic interior structure. In the study region, CTD profiles showed a stratified two-layer system. Using a two-layer finite depth model, we predicted the phase velocity of this internal wave was 0.25 m/s. The Doppler-shifted phase velocity associated with the mean flow was about 0.33 to 0.35 m/s. Therefore, the total velocity of this internal wave packet was about 0.58 to 0.60 m/s. By navigating the two SAR images to the same origin, we were able to measure the wave parameters directly from the SAR image. Intercomparison of successive SAR images suggested the internal wave packet propagated at the speed of about 0.7 m/s. Thus, the agreement between the model predicted and SAR image observed internal wave parameters was reasonable. Analysis suggested that the localized bottom topographic feature was the generating source for this internal wave packet.

ADDITIONAL INDEX WORDS: *Synthetic aperture radar, internal wave.*

INTRODUCTION

Oceanic internal waves are one of the most ubiquitous features on continental shelves (Fu and Holt, 1982). They occur in the regions of strong vertical stratification, such as the thermocline, and produced unanticipated variability in measurements made by early observers (Lafond, 1962). Just as surface gravity waves occur at the sharp density interface between the two fluids of air and water, internal waves occur where there is a sharp density change within the interior of the ocean.

It is very difficult to measure the internal wave field because it has a complex three dimensional structure and its motion is affected both by the structure of vertical stratification and by horizontal mean currents. In addition, generating sources for internal waves are not uniform. Tidal currents flowing over irregular bottom topography, atmospheric pressure fluctuations over shelf waters, surface wave interaction, barotropic tides impinging on the shelf break, *etc.*, are examples of processes which can generate internal waves.

Internal wave studies can help better understand the upper ocean dynamics and ocean interior structure (Jones, 1995). Breaking internal waves is an important mechanism for oceanic mixing (Roberts, 1976). Since internal waves are associated with the temperature and salinity structures in the upper layers of the ocean, remote sensing of internal wave patterns on the ocean surface provides additional measurements to monitor the depth of thermocline. In the coastal regions, better understanding thermocline depth is helpful for submarines and ships operations. Those facts have made internal wave study one of the most interesting topics in coastal oceanography.

In the vicinity of Cape Hatteras, North Carolina, a thin, well defined mixed surface layer exists above the seasonal thermocline on the continental shelf in the fall. This mixed layer is established by an increase in winds and a drop in air temperature, causing sea surface cooling and vertical mixing (Pietrafesa *et al.,* 1980). This creates an interface between the lighter surface water and denser deep water. Such mean vertical stratification can support the existence of internal waves which, if realized, would propagate along the density interface between the upper mixed layer and the lower layer over the adjacent continental shelf. The upper mixed layer at this time of year is usually shallow, of order a few meters in thickness. Therefore, when internal wave amplitudes are large, the local sea surface roughness will be modulated. As a result, the internal waves will have a surface expression which can be detected in a variety of remote sensing images,

---

98001 received 8 January 1998; accepted in revision 17 December 1998.

such as aerial and spacecraft photographs (Gower and Hughes, 1979; Osborne and Bruch, 1980; Zheng *et al.*, 1993), Landsat MSS (Apel *et al.*, 1975a, 1975b), and Side Looking Real Aperture Radar imagery (SLAR) (Zheng *et al.*, 1989).

Internal waves have also been detected in Synthetic Aperture Radar (SAR) images through the same mechanism (Alpers, 1983; Hughes, 1983; Kasischke, 1983; Gasparovic, 1986; Etkin, 1992). The remote sensing of ocean features with SAR depends on the interaction of microwaves and short ocean waves. As described in a review by Valenzuela (1978), experimental studies have established resonant or Bragg scattering as the most important mechanism in the interaction of an electromagnetic wave, such as a radar pulse, and the ocean surface over an incidence angle range of about 20° to 70°. The SAR imagery intensity contrasts are the result of electromagnetic field backscattered by the dynamical ocean surface, following image processing, including geometrical corrections. High resolution SAR is capable of imaging of sea surface patterns caused by, among other things, gravity waves, internal waves, ocean currents, and frontal boundaries. In the Georgia Strait experiment, Hughes and Gower (1983) used airborne SAR to obtain quantitative measurement of surface wave modulations induced by natural and ship-generated internal waves including the determination of the phase relationship between SAR image roughness variations and internal wave amplitude. In the SAR Internal Wave Signature experiment by Gasparovic *et al.* (1984), the repeat aircraft passes were used to observe the propagation of internal waves in the New York Bight. The waves were registered to the known position of a research vessel in the image, and the offsets were used to calculate propagating velocity of the internal waves. Both studies verified that sea surface manifestations of internal waves fields can be observed by SAR technology.

The study region is given in Figure 1. In this case study, two SAR images (Figure 2a and 2b), taken by the Naval Air Warfare Center (NAWC) SAR Aircraft during the Office of Naval Research High Resolution Ocean Experiment on September 16, 1991, were processed and interpreted. They were then used to infer internal wave propagation along the continental shelf off Cape Hatteras. The airborne SAR provides the unique opportunity to image the waves repeatedly in such a short period of time. This experiment coincidentally gathered oceanographic *in situ* measurements from research vessels in the region of the continental shelf in the vicinity of Cape Hatteras, specifically at 35°14′42″N, 75°9′29″W.

A packet of waves pattern was clearly seen in both images (Figure 2a and 2b) which were taken approximately 22 minutes apart. Comparison of these successive images allows direct determination of a number of basic properties of the wave packet. In addition, *in situ* measurement data are used to determine the oceanic interior structure and to derive characteristic parameters scaled for the theoretical study. By using a two layer finite depth theoretical model, the phase velocity, group velocity, were calculated and analyzed.

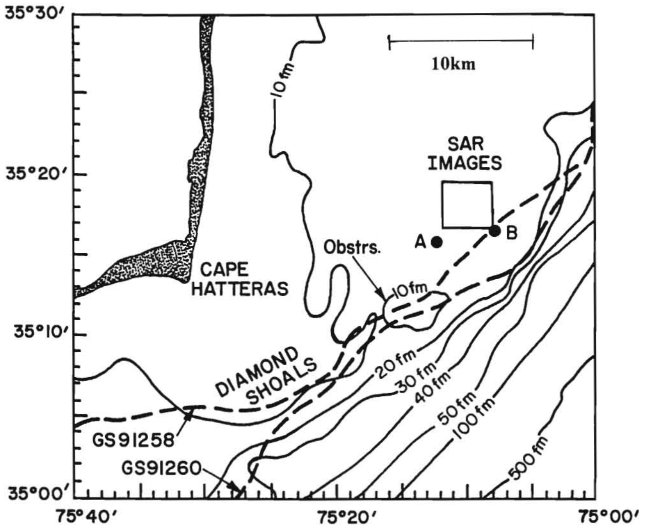

Figure 1. The locations of SAR images and R/V Bartlett's CTD stations (A and B) on U.S. Naval Oceanographic Office Bottom Contour Chart off Cape Hatteras (Map N.O. B0806). The GS91258 and GS91260 lines are the Gulf Stream north wall positions on September 15 and 17.

OBSERVATIONS

Airborne SAR Images and Interpretation

The images shown in Figure 2a and 2b were taken by the airborne NAWC SAR remote sensing system. The system has a bandwidth selectivity option for each band of either narrow bandwidth or wide bandwidth corresponding to 60 MHz or 120 MHz, respectively, and an antenna polarization selectivity option for all three bands of horizontal and/or vertical polarization on both transmit and receive. The SAR system recorded four channels of data including L-VV (L-band at a center frequency of 1.25 GHz with vertical polarization on both transmit and receive), L-HH, C-band (at a center frequency of 5.3 GHz) and X-band (at a center frequency of 9.35 GHz). The system also has a spotlight capability with the L-band. In this mode, the antenna continually repositions itself and remains trained on a particular target of interest, providing data at aspect angles ±45° from boresight. The azimuth and range resolution were 1.62 meters (m). The images presented here have been subsampled to 8 × 1.62 m. In addition, the imagery has been geometrically corrected and the backscatter intensity normalized to 45° angle of incidence. The SAR digital images were processed at Environmental Research Institute of Michigan (ERIM). Lyzenga (1998) and Lyzenga and Marmorino (1998) gave information about SAR digital processing and comparison between some SAR images imaged at different bands. In this study we focused on a group of wave patterns seen in two L-VV SAR images.

The major advantages of using airborne SAR images to analyze oceanic internal waves were very high resolution and repeatability. The SAR images used in this study have a resolution of 1.62 m in both azimuth and range direction. In addition, it was quite easy to repeat observations of features of interest. In this case, the scene of interest was reoccupied

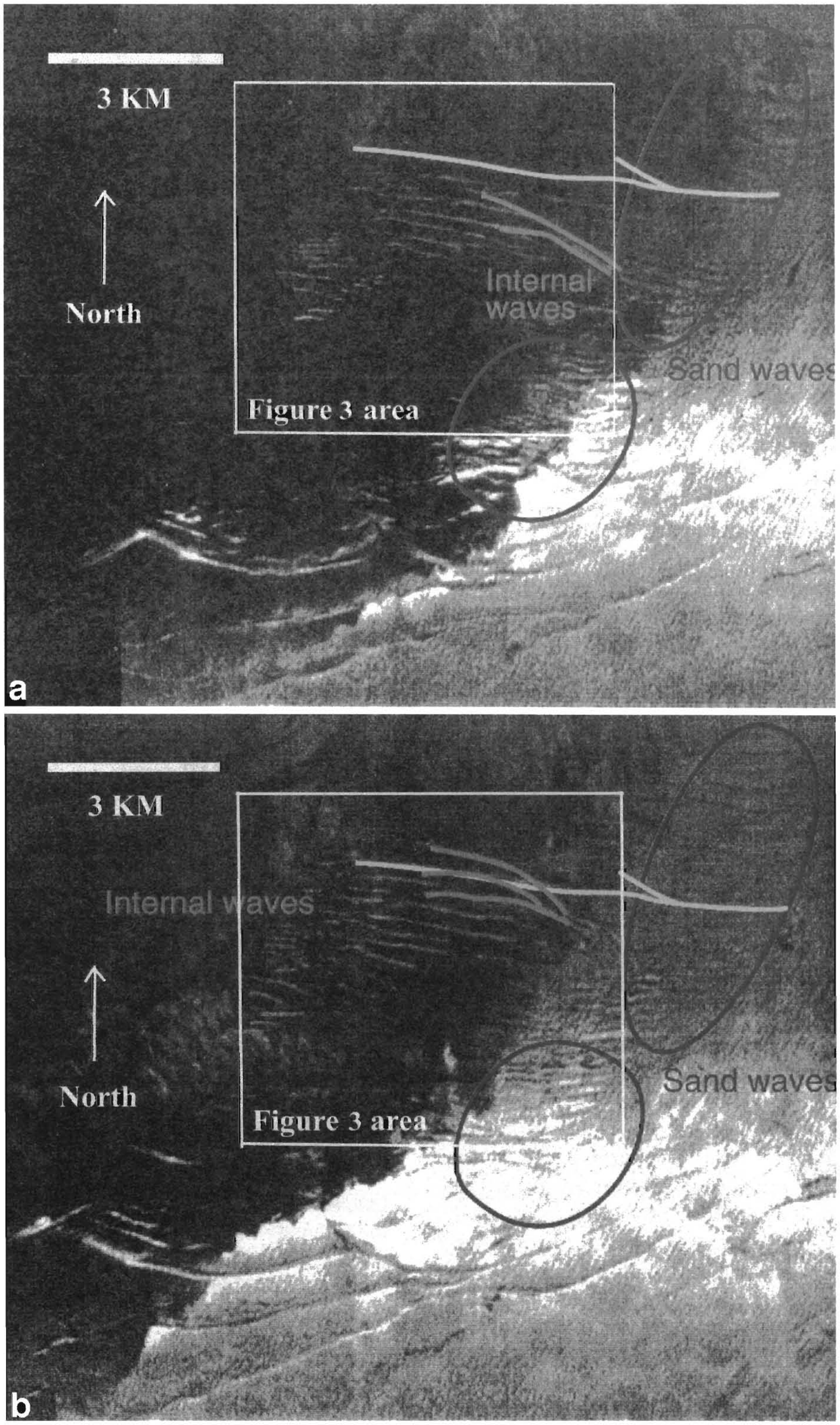

Figure 2a and 2b. Two original High-Resolution SAR images.

approximately 22 minutes after the initial imaging. Because of the precise navigation of the aircraft, it was relatively easy to geometrically correct the two SAR images and navigate them to the same origin. The bright-dark features on Figure 2a and 2b were the sea surface manifestations of internal wave and sand wave fields. In this case, it was impossible to discern the internal wave pattern from sand wave pattern, because the internal wave wavelength was comparable to that of the sand waves. However, since we navigated the two SAR images (Figure 2a and 2b) to cover the same area in the same orientation, we could compare these successive SAR images to find the moving features in the two images. From Figure 2a, we can see that that the first wave peak has a shape of bifurcation indicated by the yellow line. The bifurcation feature remains at the same position when one overlay the Figure 2a on Figure 2b. Therefore, the bifurcation marks one of the steady sand wave features. We use the bifurcation feature as our reference position (RP). There was a distinct internal wave signature to the northeast of RP on Figure 2b (green lines). The internal wave packet contains three wave crests and propagates to the northeast indicated by the number next to them. In Figure 2a, there were two wave crests orientating in the same direction. Since these wave crests moved between the two images, we conclude that they are internal wave crests. The other non-moving wavelike crests are caused by sand waves. By comparing Figure 2a and 2b, we measure the internal wave position change between the leading wave crest position of the internal wave packet indicated by the leading green lines in Figure 2a and 2b. Since the time difference between the two airborne SAR images is known, we can then calculate the internal wave propagation velocity. The calculated internal wave phase velocity from the two SAR images is about 0.7 m/s.

In Figure 3, we produce two subimages with the image center located near the wave packets in Figure 2a and 2b. Information derived from the two SAR images is summarized in Figure 3.

The SAR image intensity varies according to changes in the roughness of the surface of the ocean. In this case these changes in roughness were due to the surface expression of internal wave and sand wave features. The image intensity contrast taken along the line P1–P2 in Figure 3 (the image pixel value along P1–P2 divided by the average image pixel value) vs. distance between P1–P2 is plotted in Figure 4. Since the two SAR images have been navigated to the same origin, Points P1 and P2 are at the same location on both images. The solid and dash lines both showed that the SAR imagery readily resolved distinct waves in the packet in both images. Line P1–P2 was drawn to be approximately perpendicular to the wave crests. The image pixel size is 8 × 1.62 m by 8 × 1.62 m. Therefore, the distance between P1 and P2 can be calculated once the positions of P1 and P2 were fixed.

The average peak-to-peak wavelength (λ) of the middle eleven waves was approximately 270 m. The first and second images were taken at 16:28:00 UTC and 16:49:50 UTC, respectively. Most of the wave crests in the lower image of Figure 3 matched the wave pattern shown in upper image of Figure 3. Therefore, there is no wave propagation during the time interval between the SAR images of 22 minutes for these waves. This can also be seen in Figure 4, where the positions of wave peak along P1–P2 line in upper image match exactly those of lower image in Figure 3. DONATO *et al.* (1997) showed the sand waves existed in the same area, and the majority of the wave crests can be interpreted as standing sand wave pattern. The reason that we can not distinguish this internal wave crests from the sand wave crests in Figure 4 are that they are almost overlaid.

In summary, from these two SAR images we estimated the internal wave phase velocity to be about 0.70 m/s. In addition we measured the internal wave wavelength to be about 270 m.

In situ Measurements

During the time of the aircraft overflight, the US Navy Vessel R/V Bartlett was collecting sea truth observations. The ship surveyed the north wall of the Gulf Stream making detailed measurements of surface parameters and vertical profiles of the temperature, salinity and density fields using a conductivity-temperature-depth (CTD) profiler. The ship position, heading, wind speed, and air and sea temperatures were sampled every 10 minutes. Figure 5 shows the CTD profiles at locations A and B in Figure 1. The vertical axis pressure unit in Figure 5 was a decibar (10^4 Pa), which is approximately the hydrostatic pressure at one meter depth in sea water. These vertical profiles were taken between three and four hours after the first SAR image was recorded. Since the wind speed is low and ocean is calm during the experiment, it was reasonable to assume that the ocean interior structure did not change much over less than four hours of time. CTD profiles in Figure 5 should still be representative of the subsurface density field at the time of the overflights. The CTD profiles show a well defined two layer system in the study area with a sharp pycnocline at approximately 9 m depth. The well mixed upper layer had a thickness h_1 of 9 m and density ρ_1 of 1022 kg/m^3 (density = $\sigma_\theta + 1000$ kg/m^3, and σ_θ is the potential density). The uniform lower layer had a thickness h_2 of $H\text{-}h_1$, density ρ_2 of 1023 kg/m^3. The density difference between the two layers was $\rho_2 - \rho_1$ or $\Delta\rho$. The mean density is $(\rho_1 + \rho_2)/2$ or ρ. The depth of the water column, H, was about 35 m at this location. In addition, the observations from the ship at 16:30:00 UTC showed an air temperature of 29.94°C, a sea surface temperature about 27°C and wind speed of 1.62 m/s (at 10 meters).

TWO LAYER FINITE DEPTH MODEL

It was assumed that the flow was in the Boussinesq approximation, and the effects of the earth's rotation were neglected, *i.e.*, the Rossby number was taken as large. The vertical momentum equation used to describe the vertical motion in a stratified ocean of arbitrary Brunt-Väisälä frequency N(z) can be written (PHILLIPS, 1977) as

$$\frac{\partial^2}{\partial t^2}(\nabla^2 W) + N^2(z)\nabla_H^2 W = 0. \tag{1}$$

The wave solutions which are periodic in x and t can be sought in form $W = W(z)\exp i(KX - \omega t)$. X axis is chosen to be perpendicular to wave crest. Thus, if U is the mean veloc-

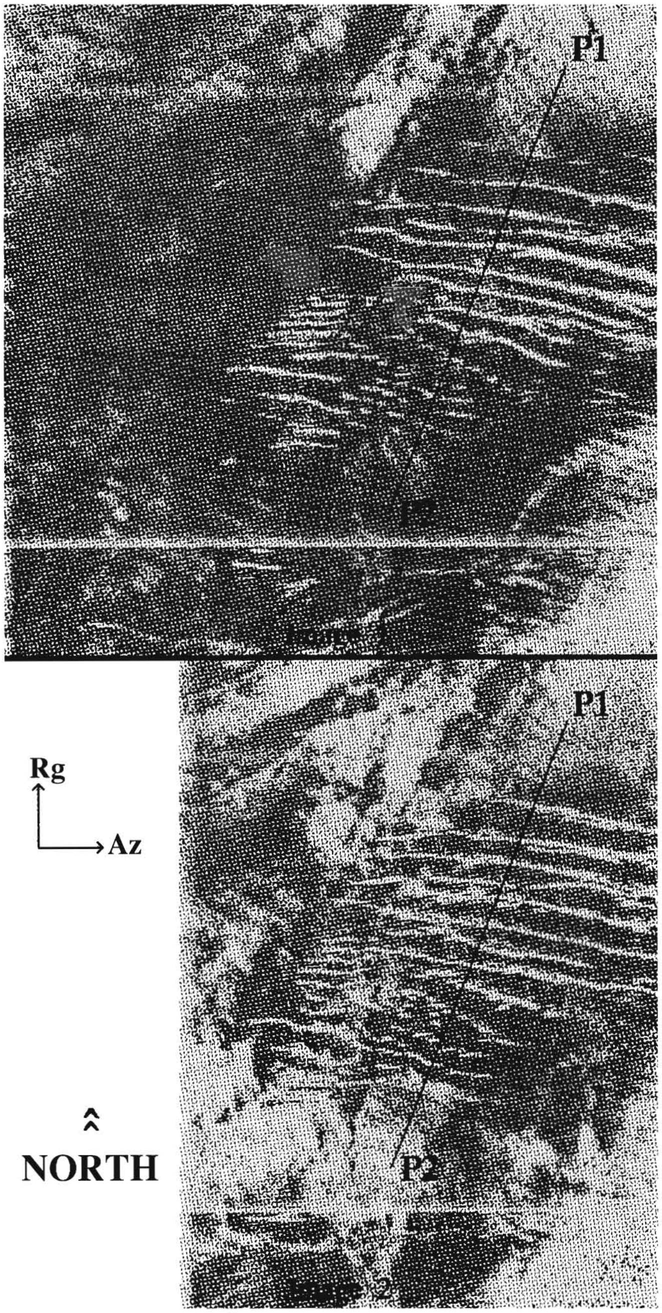

Synthetic Aperture Radar Image

EXPERIMENT NAME:
ARI HIGH RESOLUTION

Flight Date: 16-Sep-1991
Flight Time: 16:28:00 UTC (Image 1)
Flight Time: 16:49:50 UTC (Image 2)
Plot Origin: (0,0) meters
Latitude: 35.301 N°
Longitude: 75.158 W°

Image Parameters
Geometrically Corrected
Intensity Normalized to 45° Incidence
LEE filter Applied

Aircraft Parameters
Altitude: 3548 m
Heading: 89.6°

Radar Parameters
Look: Left
Frequency: L Band
Polorization: VV

Resolution:
Range: 8*1.62 m
Azimuth: 8*1.62 m

0m 1000 2000 3000m

Figure 3. Airborne SAR images of oceanic internal wave and sand wave patterns.

ity in the direction of X-axis, then $X = X_\gamma \pm Ut$, and $W = W(z)\exp i[KX - (\omega \pm UK)t]$. Substituting W into governing equation (1), we have

$$\frac{d^2W(z)}{dz^2} + \left(\frac{N(z)^2}{\sigma^2} - 1\right)K^2W(z) = 0 \qquad (2)$$

where N(z) is expressed as

$$N(z) = \left(-\frac{g}{\rho}\frac{\partial\rho}{\partial z}\right)^{1/2}. \qquad (3)$$

$\sigma = \omega \pm UK$ is the internal wave frequency, $K = 2\pi/\lambda$, is the horizontal wave number, and W(z) is the vertical velocity.

Equation (1) was solved analytically. From Figure 5, we can see that the water density changes rapidly within a small range of Δd around the pycnocline. Therefore, the Brunt-Väisälä frequency N(z) had its maximum value near the thermocline and is small at other depths.

Equation (1) can be further simplified. PHILLIPS (1977) integrated equation (1) over the range of depth Δd surrounding the thermocline. The internal boundary condition across the

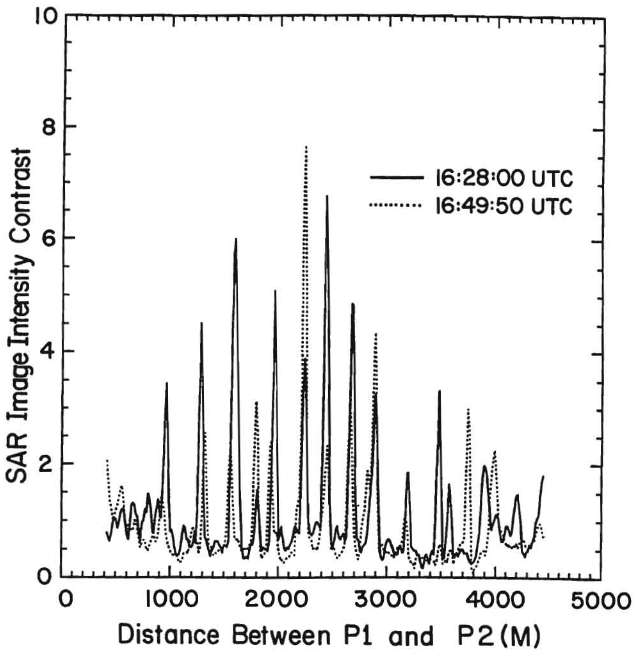

Figure 4. SAR image intensity contrast along P1 and P2.

thermocline was that the vertical velocity of the lowest internal wave mode was continuous. Because the measured internal wave wavelength (about 270 m) was fairly large compared to the water depth (30 m), the bottom boundary condition is taken as $W(-H) = 0$, and at the sea surface, the free surface boundary condition can be taken to be $W(0) = 0$ to sufficient accuracy. Equation (1), together with these boundary conditions form a second order Sturm–Liouville problem. The lowest eigenvalue satisfying the governing equation and boundary conditions leads to the dominant internal wave mode dispersion relation

$$\sigma = \pm UK + \left(\frac{K\cdot g'}{K\cdot\Delta d + \coth(K\cdot h_1) + \coth(K\cdot h_2)}\right)^{1/2} \tag{4}$$

where, g' is the reduced gravity associated with the density change across the thermocline interface, and $g' = g\Delta\rho/\rho$ where g is taken as 9.8 m/s^2. From Figure 5 we can see that Δd (a few meters) is very small compared to internal wave wavelength (270 m).

The wavelength λ of the internal waves, as determined from the SAR observations, is much greater than Δd, so that $K\Delta d \ll 1$. So, this term can be neglected in equation (3). h_1, h_2, ρ_1, ρ_2 and Δd can be determined directly from the CTD observations. Thus, all the parameters in the dispersion relation (3) are known. The wave number K ($2\pi/\lambda$) is then calculated.

The phase velocity C_p can be obtained from

$$C_p = \frac{\sigma}{K}. \tag{5}$$

C_p was found to be 0.25 m/s ± U. Unfortunately, there were no detailed currents measurement within wave field. The

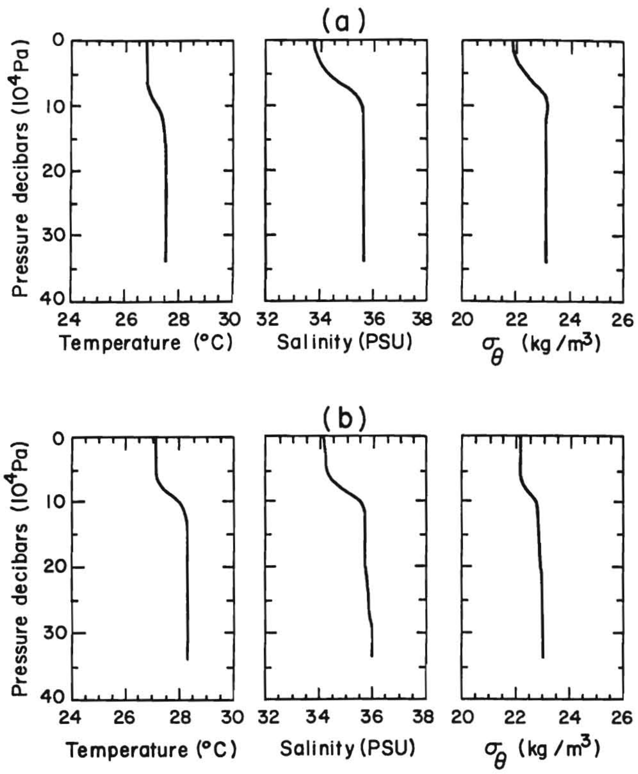

Figure 5. CTD profiles at stations A and B in Figure 1.

only simultaneously observed northward movement of a salinity front in the study area (DONATO *et al.,* 1997) showed that its velocity was about 0.3 m/s. They also showed the mean current was in the direction of northeast and its velocity was less than 0.5 m/s. The mean current direction was the same direction as that of the orientation of wave packet, which was about 25° and 30° to the east. If the salinity front movement was associated with the mean flow, then the mean current velocity was about $(0.30\ \text{m/s})/\cos(25° \sim 30°) = (0.33 \sim 0.35)$ m/s. This mean velocity was about the same as the wave propagation velocity. Therefore, the total phase velocity of the model output was about 0.58 to 0.60 m/s. This explains that the wave propagates in the speed of about 0.7 m/s measured by two SAR images.

From equation (3), after neglecting the $K\Delta d$ term, the group velocity C_g is

$$\begin{aligned} C_g &= \frac{\partial\sigma}{\partial K} \\ &= \pm U + C_p\left(\frac{1}{2} + \frac{K\cdot h_1\cdot\sinh^2(k\cdot h_2) + K\cdot h_2\cdot\sinh^2(K\cdot h_1)}{2\sinh(K\cdot h_1)\cdot\sinh K(h_1+h_2)\cdot\sinh(K\cdot h_2)}\right) \end{aligned} \tag{6}$$

C_g is found to be $0.96C_p$.

DISCUSSION

From the above calculation, the group velocity of this internal wave packet is less than the phase velocity (C_g =

0.96C$_p$). Therefore, this group of internal waves was dispersive. The wave energy dissipates with time. This observation was consistent with the earlier observations of like phenomena by ALPERS (1983), ETKINS (1992) and ZHENG (1993). In this case, C_g is very close to C_p, the dissipation is a long process. From two SAR images, we can not see the dramatic wave dissipation within 22 minutes.

ALPERS *et al.* (1983) using SEASAT SAR images, showed that internal waves were generated by the reverse tidal flow over the sill in the Strait of Messina. They found the internal wave packet propagated along the coast and parallel to the tidal flow. KASISCHKE *et al.* (1983) examined 21 passes of SEASAT SAR imagery collected over the eastern North Atlantic Ocean and found that the geographic locations of all internal wave signatures were within 10 kilometers of an ocean bottom feature, such as a seamount, a submarine ridge, a bottom obstruction, or a bank. In addition, no particular inherent propagating direction was found. In the study of internal waves on the continental slope of Middle Atlantic Bight, ZHENG *et al.* (1993) showed that the crest lines of the internal waves are nearly parallel to the bottom contours, as they were generated by the tidal flow impinging against the continental slope. These studies all confirm that the direction of internal wave propagation is related to the mean current and bottom topography.

In this study, the "Bottom Contour Chart" published by the U.S. Naval Oceanographic Office (Map N.O. B0806) is drawn in Figure 1. The depth contours unit is in fathoms (1 fm = 1.829 meter). The region that is shallower than 10 fm off Cape Hatteras is Diamond Shoals. A topographic bump exists to the north and east of the Diamond shoals, which presents obstruction to an alongshore current, but is located about D = 12 km southwest of our SAR observation area. The group velocity estimated from the two layer model, $C_g = 0.96\ C_p$, without mean current at the bump location, is about 0.24 m/s. Therefore, if the wave is generated at the bump location, then it would take D/C_g, about 13 to 14 hours to travel to the study area. It is less likely for this small scale waves to travel that long distance because of the energy dissipation for this small scale wave packet. As described in two layer finite depth model, the model is established in a non-rotating frame (Rossby number U/fL is much greater than 1, $U \sim 0.25$ m/s, $f \sim 10^{-4}$/s, $L \sim 270$ m). Therefore, this internal wave could propagate in any direction, but most likely is in the same direction as that of the mean current. From section 3, we have showed that this group of internal waves is parallel to the observed mean current.

In this area, tidal current magnitudes are much smaller than that of mean currents. The velocity is much less than that of Gulf Stream (GS). In our study region mean current is not within the Gulf Stream during the experiment period, although the GS path is spatially variable and can move laterally by tens of kilometers in a matter of a week (PIETRAFESA, 1989). The GS front location can be determined from NOAA/AVHRR data. Although these remapped AVHRR images have a spatial resolution of about 1.5 km, they still show the location of the GS during the experiment. The GS91258 and GS91260 lines on Figure 1 are the GS front positions digitized from NOAA-11 AVHRR data collected at 19:50:46 UTC on Julian day 258 (September 15, 1991) and at 19:28:04 UTC on Julian day 260 (September 17, 1991), respectively. The AVHRR images in the experiment area on September 16 are cloud covered. The Gulf Stream north wall locations show that the study region is north to Gulf Stream front. DONATO *et al.* (1997) showed that there exists a group of sand waves with magnitudes of about 2 m in the study region, and in the same direction of the wave crest, which suggests that irregular bottom topography could be the generating source for this internal wave packet.

CONCLUSION

SAR imagery can provide significant information for the study of internal waves. Two airborne SAR images collected during the High Resolution Ocean Experiment (VALENZUELA, 1991) showed a well-defined oceanic internal wave pattern propagating on the continental shelf off Cape Hatteras. The dominant wavelength and propagation direction of the internal waves can be measured directly from the SAR images. The phase velocity can also be measured through intercomparison of successive SAR images. In this case study, the representative wavelength of the internal waves was observed to be about 270 m and the waves were propagating with phase speeds of 0.7 m/s and in a northeastward direction, parallel to the Gulf Stream path.

Information derived from both the SAR imagery and coincident *in situ* oceanographic measurements were used in a dynamical ocean model to derive the dominant wave parameters for internal waves. The internal wave phase velocity derived from the two-layer, finite depth-model is found to be 0.25 m/s. If we consider the Doppler shift associated with the mean flow, the actual internal wave velocity is about 0.58 to 0.60 m/s. Thus the model agrees quite well with that obtained directly from SAR images. In addition, the localized bottom sand wave pattern appears to be the generating source for this wave packet. In this case, the phase velocity bias between the model output and the SAR measurements is partially due to the lack of the detailed current velocity data to estimate the accurate Doppler shift. The current measurement is needed in the future study in order to determine the interaction between the internal wave field and local currents.

ACKNOWLEDGMENTS

This work was supported under the Naval Air Warfare Center contract N 62269-92-M-3483 (J. M. Morrison) and the US Department of Energy grant DEFG 05-95-ER62053 (L. J. Pietrafesa). The authors would like to express their appreciation to R. Gasparovic for suggestions that helped to improve this paper. The CTD data were collected aboard the USNS Bartlett under the direction of G. Marmorino (Chief Scientist) and as a part of the Naval Research Laboratory (NRL) High Resolution Remote Sensing ARI, and were kindly provided to us by the NRL. L. Salzillo and P. Davis prepared Figures. L. Gray and B. Batts did the word processing. We also would like to thank two anonymous reviewers for their helpful comments.

LITERATURE CITED

ALPERS, W. and SALUSTI, E., 1983. Scylla and Charybdis observed from space. *Journal Geophysical Research,* 88, 1,800–1,808.

APEL, J.R.; BYRNE, H.M.; PRONI, J.R., and CHARNELL, R.L., 1975a. Observations of oceanic internal and surface waves from Earth Resources Technology Satellite. *Journal Geophysical Research,* 80, 865–881.

APEL, J.R.; PRONI, J.R.; BYRNE, H.M., and SELLERS, R.L., 1975b. Near-simultaneous observations of intermittent internal waves on the continental shelf from ship and spacecraft. *Geophysical Research Letters,* 2, 128–131.

DONATO, T.; ASKARI, F.; MARMORINO, G.O.; TRUMP, C.L., and LYZENGA, D.R., 1997. Radar imaging of sand waves on the continental shelf east of Cape Hatteras, NC, USA. *Continental Shelf Research,* 9, 989–1004.

ETKIN, V.S. and SMIRNOY, A.V., 1992. Observations of internal waves in ocean by radar methods. *IEEE,* 143–145.

FU, L.L. and HOLT, B., 1982. Seasat views oceans and sea ice with synthetic-aperture radar. *JPL Publication* 81–120.

GASPAROVIC, R.F.; APEL, J.R., and KASISCHKE, E.S., 1988. An overview of the SAR Internal Wave Signature Experiment. *Journal Geophysical Research,* 10, 12,304–12,316.

GASPAROVIC, R.F.; APEL, J.R.; THOMPSON, D.R., and TOCHKO, J.S., 1986. A comparison of SIR-B synthetic aperture radar data with ocean internal wave measurements. *Science,* 232, 1,529–1,531.

GOWER, J.F.R. and HUGHES, B.A., 1979. Radar and ship observations of coastal sea surface roughness patterns in the Gulf of Georgia, *Proc. Thirteen Int. Symp. Remote Sens. Environ.,* pp. 103–115.

HUGHES, B.A., and GOWER, J.F.R., 1983. SAR imagery and surface truth comparisons of internal waves in Georgia Strait, British Columbia, Canada, *Journal Geophysical Research,* 88, 1,809–1,824.

JONES, R.M., 1995. On using ambient internal waves to monitor Brunt-Väisälä frequency, *Journal Geophysical Research,* 100, 11,005–11,011.

KASISCHKE, E.S.; TSENG, Y.C.; MEADOWS, G.A., and LIU, A.K., 1983. Observations of internal waves and frontal boundaries on SEASAT SAR imagery collected over the eastern North Atlantic Ocean. *Seventeenth International Symposium on Remote Sensing of Environment.* (Ann Arbor)

LAFOND, E.C., 1962. *Internal Waves, The Sea,* Vol. 1, edited by M.N. Hill, pp. 731–751, New York, Wiley.

LYZENGA, D.R., 1998. Effects of intermediate-scale waves on radar signatures of ocean fronts and internal waves. *Journal Geophysical Research,* 103, 18759.

LYZENGA, D.R. and MARMORINO, G.O., 1998. Measurement of surface currents using sequential synthetic aperture radar images of slick patterns near the edge of the Gulf Stream. *Journal Geophysical Research,* 103, 18769.

OSBORNE, A.R. and BURCH, T.L., 1980. Internal solitons in the Andaman Sea. *Science,* 208, 451–460.

PHILLIPS, O.M., 1977. *The dynamics of the upper ocean.* Cambridge: Cambridge University Press.

PIETRAFESA, L.J. and JANOWITZ, G.S., 1980. On the dynamics of the Gulf Stream front in the Carolina Capes. *Stratified Flows: the Second International Symposium on Stratified Flows,* Tapen Publishing Company, pp. 184–197.

PIETRAFESA, L.J., 1989. The Gulf Stream and wind events on the Carolina capes Shelf. *National Undersea Research Program Research Report 89-2.* North Carolina Coastal Oceanography Symposium, 89–129.

ROBERTS, J., 1975. *Internal Gravity Waves in the Ocean.* New York, Marcel Dekker.

VALENZUELA, R.G., 1978. Theories for the interaction of Electromagnetic and ocean waves—A review. *Boundary Layer Meteorology,* 13, 61–85.

VALENZUELA, G.R., 1991. Operations plan for High-Resolution 1 Experiment. Code 4243, Naval Research Laboratory.

ZHENG, QUANAN; WU, LONGYE; ZHANG, DONG, and LI, XIAOFENG, 1989. A study on SLAR image signatures of internal waves in the sea area nearby the Laoshan Bay. *Oceanol. Limnol. Sinica,* 20, 281–287.

ZHENG, QUANAN; YAN, XIAO-HAI, and KLEMAS, VIC, 1993. Statistical and dynamical analysis of internal waves on the continental shelf of the Middle Atlantic Bight from space shuttle photographs. *Journal Geophysical Research,* 98, 8,495–8,504.